A Distributed Radar and Communication System with Interference Cancellation and Power Control

Adham Sakhnini, André Bourdoux, Sofie Pollin

Abstract—We present a distributed *cell-free* communication and radar system that operates in the uplink. The system schedules dedicated transmit (Tx) access points (APs) to transmit dedicated radar signals in the uplink together with the user equipment (UE). The receiving (Rx) APs decode the UE payloads while also detecting targets based on the Tx AP signals. To mitigate the added Tx AP interference, the Rx APs use multiuser processing to recover the UE payloads, while a combination of large processing gains, adaptive beamforming, spatial diversity, interference cancellation and power control is used to mitigate the UE interference impacting the radar. The radar introduces few changes to the physical layer and the additional computations needed are comparable to the communication system. The system is validated numerically by using Monte-Carlo simulations, where we highlight the inherent trade-offs between the various system parameters (such as the power control balancing, and the number of Tx APs scheduled and UEs cancelled) and show that both the communication and radar systems can be effectively integrated into the same network at a near optimal performance.

Index Terms—Communication, radar, cell-free, distributed, interference cancellation, power control, spatial diversity

I. INTRODUCTION

The framework of distributed *cell-free* communication networks has emerged as a promising technology for future wireless communication standards [1]. The concept is an extension of previous systems by synchronously and phase coherently operating a large number of distributed antennas throughout a coverage area. This has the impact of providing a uniform and reliable service to the user equipment (UE) thanks to the favorable propagation and channel hardening effects [2].

Another technology envisioned in future standards is the integration of radar systems into the wireless infrastructure [3], [4]. The grand vision is to integrate radar sensing into the same hardware, signal processing, waveforms and protocols without impacting the communication system. The main motivations include improved spectrum utilization and the enabling of new applications and services related to the radar sensing, while potentially feeding the output back to the communication system to mutually improve the performance.

The topic of radar and cell-free networks has recently received significant attention in the literature [5]–[19]. These networks consist of distributed access points (APs) that serve the UEs in a time-division duplex (TDD) schedule, where the uplink channel estimates are used to serve the UEs in the downlink through channel reciprocity. In order to integrate the radar system, most works partition the APs into transmit (Tx) APs that transmit dedicated radar waveforms and receive (Rx) APs that perform the radar processing (cf. [5]–[16]). When full-duplex is assumed [17]–[19], then the same APs used for downlink transmission also receive the echoes reflected from

the environment (these setups can be considered as a special case where the Tx and Rx APs are collocated). To this end, the works can be largely categorized by the transmission scheme employed, where we distinguish the radar operating in the *downlink* [5]–[13], [17]–[19] from the *uplink* [14]–[16].

The downlink integrations operate by allocating dedicated precoders for the radar system, where the performance trade-offs are primarily balanced with power control or direct optimization of the precoders [5]–[13], [17]–[19]. In these schemes, the Tx APs transmit payloads to the UEs while also scanning the environment with the radar beams. The UEs receive and decodes the payloads while the Rx APs perform radar on the reflected echoes. The works in [5]–[8], [17], [18] develop various precoding and power control schemes to optimize the total performance, and the additional problem of partitioning the APs into Tx and Rx APs is considered in [9], [10]. Security aspects in the presence of eavesdroppers are considered in [11], [12], [19], and energy efficiency and low latency communications is considered in [13]. To this end, the main cost of operating in the downlink is a loss in transmit power allocated to the radar beams, interference between the UE and radar precoders and, unless full-duplex is assumed, the loss of one Tx AP for each allocated Rx AP.

The works in [14]–[16] consider the uplink by scheduling the Tx APs to transmit dedicated radar signals together with the UEs in the uplink. The Rx APs receive both the radar and UE signals and perform both payload decoding and radar sensing. The works in [14] and [15] consider the payload segment by developing combining filters and power control schemes, while [16] considers the pilot segment. The choice of using the training or payload segments depends on the channel conditions; the pilots allow for an improved interference rejection, while the payload offers a higher integration gain as more data is available. Similar to the downlink, the cost involves interference between the Tx APs and the UEs, and the loss of one Tx AP for each allocated Rx AP (unless full-duplex is assumed). However, there is no loss in transmit power as the Tx APs only transmit radar signals.

To this end, there are several hardware related challenges involved in the realization of cell-free networks. These appear to be the main implementation bottlenecks and include managing the fronthaul capacity, establishing phase coherency, and synchronizing and coordinating the APs [1]. These bottlenecks also appear in distributed radar systems, and may in some cases be more challenging than for the communication system. For example, a time alignment of less than a microsecond across the APs is often sufficient in a communication system, as the offsets fall within the cyclic prefix of most waveforms. In contrast, radar systems require nanosecond accurate timing

between the APs in order to implement ranging. This is because one nanosecond correspond to 30 cm in bistatic range, while one microsecond corresponds to 300 m.

A similar imbalance occurs in radar systems that employ distributed beamforming (or combining), as these systems not only require phase *coherence*, but also phase *alignment*, which is a stricter form of synchronization that also requires a calibration of the radio front-ends. Another difficulty is the need to estimate the AP locations and their relative orientations. While this is not strictly needed for communications, it is a fundamental requirement for radar systems in order to determine the locations of the targets. Fortunately, estimates can often be obtained during deployment, which may be sufficient for multistatic radar networks. However, it is more challenging in distributed beamforming systems, as the relative antenna locations must be sufficiently accurate for the waveforms to align phase coherently at the destination, implying wavelength level accuracy. The consequence of these effects is a possible imbalance at the system level, where the radar integration requires *more* than what the infrastructure may support.

While this paper does not solve all of these issues, it proposes a radar integration that has relatively mild requirements on the infrastructure. The system operates in the uplink of the TDD frame and is an extension of our previous work in [14], [15]. The APs are split into Tx and Rx APs, where the Tx APs transmit dedicated signals for sensing and the Rx APs receive both the radar and UE signals. Phase coherency is assumed for the processing of the UEs (this is necessary for cell-free systems), but phase alignment is not a requirement. Furthermore, coarse estimates of the antenna locations and orientations are assumed throughout the paper. These are not *strictly* needed for the radar processing, but are required post-detection for assigning locations to the targets. This does not require wavelength level accuracy and can potentially be obtained together with the timing offsets with multiple-input multiple-output (MIMO) radar processing [20].

Since the Tx APs and the UEs transmit at the same time, the main challenge is to manage the mutual interference. From the communication point of view, the Tx APs can be treated as conventional UEs and mitigated natively with multiuser processing at the Rx APs. In contrast, the UE interference impacting the radar is more severe as it rapidly degrades the detection performance. This is because the radar is required to detect weak targets buried in the noise and therefore requires a high receiver sensitivity. Hence, in order to mitigate the interference, we leverage a total of five degrees freedom:

1) *Large processing gains* to increase the signal to interference plus noise ratio (SINR).
2) *Adaptive beamforming* to spatially suppress the UE interference in the antenna domain.
3) *Interference cancellation* to suppress the UE interference in the subcarrier domain.
4) *Spatial diversity* to compensate blind regions, thanks to the large variations in aspect angles across the APs.
5) *Power control* to balance the trade-offs in communication and radar performance.

These are further described as they are presented throughout the paper, and also summarized in Section VI.
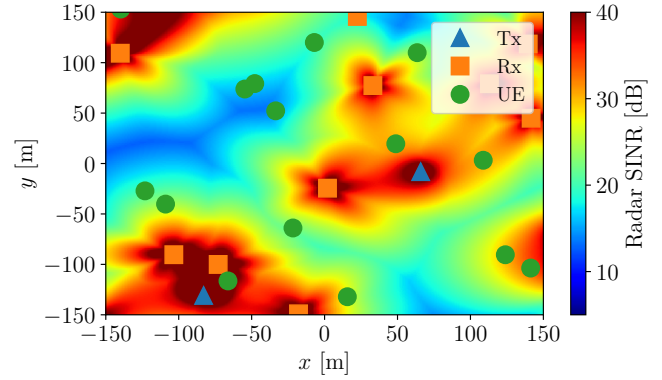

Figure 1: A simulated SINR radar map of the proposed system, which consists of UEs and APs operating in a cell-free architecture. In order to facilitate sensing, the APs are split into Tx and Rx APs. The Tx APs transmit dedicated signals for sensing while the Rx AP receive both the UE and Tx AP signals. Since the Tx APs operate like the UEs, the increase in system load is handled *natively* with multiuser processing at the Rx APs. From the radar point of view, the UEs act as interferers that limit the detection performance. This is mitigated by leveraging a combination of large processing gains, adaptive beamforming, spatial diversity, power control and interference cancellation.

A significant advantage of the system is the uniform transmission employed for target detection. This means that the Tx APs transmit isotropically so that a wide area coverage is achieved without the need for beam scanning, allowing for a fast update rate and high Doppler resolution [21]. Interestingly, this also provides a direct synergy with the previous works that employ downlink beamforming [5]–[13], [17]–[19], as the detections in the uplink can be used to direct the downlink beamformers on the targets without the need to exhaustively scan the environment. This allows the network to operate in dual mode, where the uplink *detects* and the downlink *tracks* the targets, reminiscent of multi-mode radar systems.

An example of the proposed system is illustrated in Fig. 1, which shows a simulated SINR map of the radar system under the presence of UEs. As can be seen, by selecting a small numbers of Tx APs, a large coverage can be achieved thanks to the large number of Rx APs. Although the performance depends on a large number of parameters, such as the Tx and Rx AP partitioning, power control and various signal processing and system parameters, we show by using Monte-Carlo simulations that a *per-frame* radar coverage of 93.5% can be achieved at the cost of 8.7 to 18.2% in spectral efficiency (SE) when cancelling at least 8 UEs at each Rx AP in a 500×500 meter service area consisting of 32 APs and 40 UEs at random locations. Depending on the scheduling priority, the performance can easily be tuned to favor either the UEs or the Tx APs with the power control.

The paper is organized as follows: Section II presents the signal model, and Section III and IV present the signal processing. The problem of resource allocation is considered in Section V and the system is then evaluated in Section VI.

II. SIGNAL MODEL

We consider U UEs and M APs, where each UE has a single antenna and each AP has N antennas. The orthogonal frequency division multiplexing (OFDM) waveform is used, where K denotes the number of subcarriers and L the number of symbols in a processing frame. The set of APs is denoted by $\Omega = \{1, 2, ..., M\}$ and in order to sense the environment, a subset $\mathcal{T} \subset \Omega$ of Tx APs are used to transmit dedicated radar signals in the uplink. These signals share same time-frequency resources as the U UEs and are additionally received by the remaining Rx APs. The Tx APs are selected from the APs in the network and are assumed to operate with single antennas like the UEs. Full-duplex is not assumed, so that when an AP is allocated for sensing as a Tx AP, it cannot be used as an Rx AP for processing the uplink communication signals.

The received OFDM demodulated signal $\boldsymbol{y}_m(k, l) \in \mathbb{C}^N$ at Rx AP $m \in \Omega/\mathcal{T}$, subcarrier k and symbol l is modeled as

$$\boldsymbol{y}_m(k, l) = \boldsymbol{y}_m^{(r)}(k, l) + \boldsymbol{y}_m^{(c)}(k, l) + \boldsymbol{e}_m(k, l) \qquad (1)$$

where $\boldsymbol{y}_m^{(r)}(k, l)$ is the radar signal originating from the Tx APs and $\boldsymbol{y}_m^{(c)}(k, l)$ is the communication signal from the UEs. The noise $\boldsymbol{e}_m(k, l) \in \mathcal{CN}(\boldsymbol{0}, \sigma^2 \boldsymbol{I}_N)$ is a zero mean and complex Gaussian random variable with variance σ^2.

A. The radar signal

The radar signal is composed of the sum of uplink transmissions from the Tx APs and is expressed as

$$\boldsymbol{y}_m^{(r)}(k, l) = \sum_{n \in \mathcal{T}} \sqrt{p_n^{(r)}} \boldsymbol{g}_{m,n}(k, l) s_n^{(r)}(k, l) \qquad (2)$$

where $p_n^{(r)}$ is the Tx power and $s_n^{(r)}(k, l)$ is the radar payload of Tx AP n, and $\boldsymbol{g}_{m,n}(k, l)$ is the radar channel between Rx AP m and Tx AP n. The radar channel is modeled as a superposition of Q point scatterers (or targets) as

$$\boldsymbol{g}_{m,n}(k, l) = \sum_{q=1}^{Q} \alpha_{m,n,q} \boldsymbol{v}_{m,n,q}(k, l) \qquad (3)$$

where $\alpha_{m,n,q}$ is the complex amplitude of target q and $\boldsymbol{v}_{m,n,q}(k, l) \in \mathbb{C}^N$ is the corresponding space-time-frequency steering vector, which is given by

$$\boldsymbol{v}_{m,n,q}(k, l) = \boldsymbol{b}_m(\theta_{m,q}) e^{j2\pi \frac{\Delta f d_{m,n,q}}{c} k} e^{-j2\pi \frac{cT_p \nu_{m,n,q}}{f_c} l} \qquad (4)$$

where $\boldsymbol{b}_m(\theta) \in \mathbb{C}^N$ is the steering vector of AP m with respect to the direction of arrival (DOA) θ, $\theta_{m,q}$ is the DOA between AP m and target q, and $d_{m,n,q}$ is the bistatic distance and $\nu_{m,n,q}$ is the Doppler velocity of target q with respect to AP m and n. The symbol duration is denoted by T_p, the speed of light by c and the carrier frequency by f_c.

B. The communication signal

The communication signal is modeled as the sum of the U signals transmitted from each UE as

$$\boldsymbol{y}_m^{(c)}(k, l) = \sum_{u=1}^{U} \sqrt{p_u} \boldsymbol{h}_{m,u}(k, l) s_u(k, l) \qquad (5)$$

where p_u is the Tx power of UE u, $\boldsymbol{h}_{m,u}(k, l)$ is the channel between UE u and AP m and $s_u(k, l)$ is the corresponding data payload, which has a zero mean and unit variance.

It holds from $\boldsymbol{y}_m^{(c)}(k, l)$ and $\boldsymbol{y}_m^{(r)}(k, l)$, that the Tx APs and UEs can be expressed with a common model as

$$\boldsymbol{y}_m(k, l) = \sum_{u=1}^{U+|\mathcal{T}|} \sqrt{p_u} \boldsymbol{h}_{m,u}(k, l) s_u(k, l) + \boldsymbol{e}_m(k, l) \qquad (6)$$

where $\boldsymbol{h}_{m,u}(k, l) = \boldsymbol{g}_{m,n_u}(k, l)$ and $s_u(k, l) = s_{n_u}^{(r)}(k, l)$ for the indices $u > U$, where the index n_u selects Tx AP n_u in $\mathcal{T}$ in some arbitrary order. This enumeration has the benefit of simplifying the communication analysis, as the Tx APs can be viewed as additional UEs imposing a load on the system. This means that the analysis of the communication system follows the same procedure as a conventional system.

The covariance matrix of the channel $\boldsymbol{h}_{m,u}(k, l)$ is denoted as $\boldsymbol{R}_{m,u}$ and the large scale fading (LSF) coefficient $\beta_{m,u}$ is defined by the average trace of $\boldsymbol{R}_{m,u}$ as

$$\beta_{m,u} = \frac{1}{N} \text{Tr}\{\boldsymbol{R}_{m,u}\} \qquad (7)$$

where Tr denotes the trace operator. It holds that $\boldsymbol{R}_{m,u}$ and $\beta_{m,u}$ can be estimated with a low overhead (as discussed in e.g., [22]) and are therefore, together with the noise power σ^2 assumed to be known throughout the paper.

III. COMMUNICATION SIGNAL PROCESSING

A. Channel estimation

The communication system starts by estimating the channels of the UEs and the Tx APs. This is done by assigning a pilot of length τ_p to each of the transmitters. These pilots are spread across the coherence blocks of the processing frame and are denoted by $\boldsymbol{\phi}_u \in \mathbb{C}^{\tau_p}$, where $\boldsymbol{\phi}_u^H \boldsymbol{\phi}_{u'} = \tau_p$ when $u = u'$ and $\boldsymbol{\phi}_u^H \boldsymbol{\phi}_{u'} = 0$ when $u \neq u'$. In order to accommodate pilot contamination, we let $\mathcal{P}_u$ denote the set of UEs and Tx APs that have been assigned the same pilot as UE u. This set is always non-empty as it also includes UE u (i.e., $u \in \mathcal{P}_u$).

The pilots are transmitted with the power $p_u^{(t)}$ by each UE and Tx AP at the assigned time-frequency resources. Once received, the training data is de-spread by using the pilot sequence $\boldsymbol{\phi}_u$ for each UE and Tx AP, resulting in

$$\boldsymbol{z}_{m,u}(k, l) = \sum_{u' \in \mathcal{P}_u} \sqrt{p_u^{(t)}} \boldsymbol{h}_{m,u'}(k, l) + \frac{1}{\sqrt{\tau_p}} \boldsymbol{e}_m(k, l) \qquad (8)$$

for the subcarriers k and OFDM symbols l that are allocated for channel estimation. The minimum mean squared error (MMSE) channel estimates are obtained from $\boldsymbol{z}_{m,u}(k, l)$ as

$$\hat{\boldsymbol{h}}_{m,u}(k, l) = \sqrt{p_u^{(t)}} \boldsymbol{R}_{m,u} \boldsymbol{\Psi}_{m,u}^{-1} \boldsymbol{z}_{m,u}(k, l) \qquad (9)$$

where $\boldsymbol{\Psi}_{m,u} = \sum_{u' \in \mathcal{P}_u} p_u^{(t)} \boldsymbol{R}_{m,u'} + \frac{1}{\tau_p} \sigma^2 \boldsymbol{I}_N$. The corresponding probability distribution is given by

$$\hat{\boldsymbol{h}}_{m,u}(k, l) \sim \mathcal{CN}(\boldsymbol{0}, p_u^{(t)} \boldsymbol{R}_{m,u} \boldsymbol{\Psi}_{m,u}^{-1} \boldsymbol{R}_{m,u}). \qquad (10)$$

The channel estimation errors are given by $\tilde{\boldsymbol{h}}_{m,u}(k, l) = \boldsymbol{h}_{m,u}(k, l) - \hat{\boldsymbol{h}}_{m,u}(k, l)$ and have the distribution

$$\tilde{\boldsymbol{h}}_{m,u}(k, l) \sim \mathcal{CN}(\boldsymbol{0}, \tilde{\boldsymbol{R}}_{m,u}) \qquad (11)$$
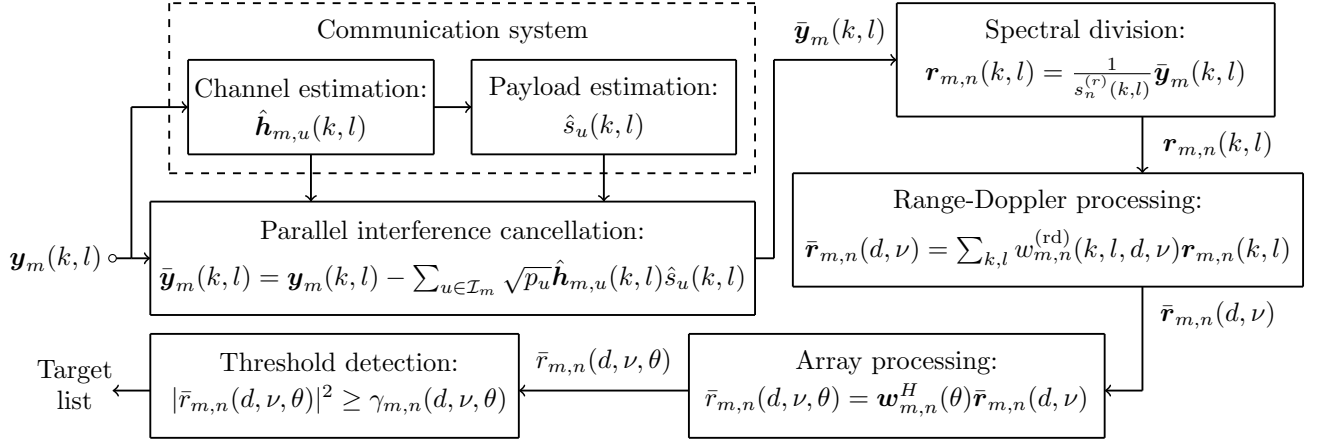
Figure 2: A high-level block-diagram of the communication and radar signal processing. The radar system makes use of the channel and payload estimates of the communication system to cancel the UE interference. The presence of a potential target at the bistatic distance d, Doppler velocity ν and steering angle θ is then evaluated for detection.

where the error covariance matrix is given by

$$\tilde{\boldsymbol{R}}_{m,u} = \boldsymbol{R}_{m,u} - p_u^{(t)} \boldsymbol{R}_{m,u} \boldsymbol{\Psi}_{m,u}^{-1} \boldsymbol{R}_{m,u}. \tag{12}$$

Note that because $\boldsymbol{R}_{m,u}$ and σ^2 are assumed known, it holds that $\tilde{\boldsymbol{R}}_{m,u}$ and $\boldsymbol{\Psi}_{m,u}$ are also known.

Since the channel estimates constitute a small fraction of the available subcarriers, we will make the strong (but for the analysis necessary) assumption that the statistical accuracy is retained across *all* subcarriers and symbols during a processing frame. This is a common assumption in the literature (see e.g., [2]) and requires that the coherence time and bandwidth is sufficiently small, and that channel tracking (and/or interpolation) is used to accommodate channel variations. Note that the assumption does necessarily mean that the performance is overestimated, as the channel estimates may also *improve* when channel tracking is used. In this sense, the assumption constitutes a middle-ground on the expected performance.

B. Payload estimation

The *soft* payload estimate $\hat{s}_u^{(s)}(k,l)$ of UE u at subcarrier k and OFDM symbol l is obtained by the weighted average

$$\hat{s}_u^{(s)}(k,l) = \sum_{m \in \mathcal{C}_u} \boldsymbol{w}_{m,u}^H(k,l) \boldsymbol{y}_m(k,l) \tag{13}$$

where $\boldsymbol{w}_{m,u}(k,l)$ is a combining filter and $\mathcal{C}_u \subset \Omega/\mathcal{T}$ is the set of APs that serve UE u. Subsequently, the communication system applies a hard decision to obtain the symbol estimates $\hat{s}_u(k,l)$. This constitutes the decoded data payload and can be obtained after e.g., forward error correction.

For the analysis, we will use the SINR of the soft payload estimates in order to assess the performance, given by

$$\text{SINR}_u(k,l) = \frac{\sum_{m \in \mathcal{C}_u} p_u |\boldsymbol{w}_{m,u}^H(k,l) \hat{\boldsymbol{h}}_{m,u}(k,l)|^2}{\sum_{m \in \mathcal{C}_u} |\boldsymbol{w}_{m,u}^H(k,l) \bar{e}_{m,u}(k,l)|^2} \tag{14}$$

where $\bar{e}_{m,u}(k,l)$ is the effective noise, which is given by $\bar{e}_{m,u}(k,l) = \sum_{i=1}^{U+|\mathcal{T}|} p_i \boldsymbol{h}_{m,i}(k,l) - p_u \hat{\boldsymbol{h}}_{m,u}(k,l) + \boldsymbol{e}_m(k,l)$ and takes channel estimation errors, UE interference, radar interference and additive noise into account.

Since the SINR depends on the subcarrier and symbol, we will consider the expected SINR which is given by

$$\text{SINR}_u = \mathbb{E}\{\text{SINR}_u(k,l)\} \tag{15}$$

and can be evaluated by Monte-Carlo simulations by averaging over the subcarriers k and symbols l. The performance depends on the choice of combiner $\boldsymbol{w}_{m,u}(k,l)$, where a common choice is the MMSE combiner (cf., [2], [23]).

IV. RADAR SIGNAL PROCESSING

The radar processing is outlined in Fig. 2. The first block constitutes parallel interference cancellation, where the channel and payload estimates of the UEs are used to reconstruct the communication signals in order to cancel the UE interference. The processing then follows by spectral division, range-Doppler processing, array processing and threshold detection. The corresponding output of the radar system is a target list which contains the parameters of the detected targets.

A. Parallel interference cancellation

The channel estimates $\hat{\boldsymbol{h}}_{m,u}(k,l)$ and payload estimates $\hat{s}_u(k,l)$ generated by the communication system are first used to cancel the communication interference by subtracting the reconstructed UE signals from the received data as

$$\bar{\boldsymbol{y}}_m(k,l) = \boldsymbol{y}_m(k,l) - \sum_{u \in \mathcal{I}_m} \sqrt{p_u} \hat{\boldsymbol{h}}_{m,u}(k,l) \hat{s}_u(k,l) \tag{16}$$

$$= \boldsymbol{y}_m^{(r)}(k,l) + \sum_{u=1}^{U} \sqrt{p_u} \boldsymbol{\epsilon}_{m,u}(k,l) + \boldsymbol{e}_m(k,l) \tag{17}$$

where $u \in \mathcal{I}_m$ is the set of UEs cancelled at AP m and $\boldsymbol{\epsilon}_{m,u}(k,l)$ is the residual UE interference. We will make the assumption that the symbol error rates are negligible (this is reasonable when error correction codes are used) so that $\hat{s}_u(k,l) = s_u(k,l)$. This gives the UE interference

$$\boldsymbol{\epsilon}_{m,u}(k,l) = \begin{cases} \boldsymbol{h}_{m,u}(k,l) s_u(k,l) & u \notin \mathcal{I}_m \\ \tilde{\boldsymbol{h}}_{m,u}(k,l) s_u(k,l) & u \in \mathcal{I}_m \end{cases} \tag{18}$$

where it holds that $\epsilon_{m,u}(k,l) \sim \mathcal{CN}(\mathbf{0}, \tilde{\mathbf{R}}_{m,u})$ for $u \in \mathcal{I}_m$ and $\epsilon_{m,u}(k,l) \sim \mathcal{CN}(\mathbf{0}, \mathbf{R}_{m,u})$ for $u \notin \mathcal{I}_m$.

The level of cancellation can be quantified by using the effective LSF coefficient $\tilde{\beta}_{m,u}$, which is given by

$$\tilde{\beta}_{m,u} = \frac{1}{N} \text{Tr}\left\{\tilde{\mathbf{R}}_{m,u}\right\} \equiv \gamma_{m,u}\beta_{m,u} \tag{19}$$

where $\gamma_{m,u}$ quantifies the *reduction* in UE interference after cancellation. If $\gamma_{m,u} = 0$, then the interference of UE u at AP m is perfectly cancelled, and if $\gamma_{m,u} = 0.5$, then the power is reduced by 50%, or equivalently 3 dB.

Note that because $\tilde{\mathbf{R}}_{m,u}$ is known, $\tilde{\beta}_{m,u}$ is also known. Consequently, it holds that $\gamma_{m,u}$ can be obtained as $\gamma_{m,u} = \tilde{\beta}_{m,u}/\beta_{m,u}$. This means that $\gamma_{m,u}$ can be assessed *before* the cancellation based on the LSF statistics and therefore taken into account during the resource allocation (cf. Section V).

Since the UE channels are directional (or spatially correlated), the cancellation level $\gamma_{m,u}$ depends on the relative location of all UEs that share the same pilots with respect to AP m. Although a simple closed form expression appears to be difficult to establish in general, it is possible to express $\gamma_{m,u}$ in closed form when the APs have only one antenna (i.e., $N = 1$) by directly evaluating (19). This gives the expression

$$\gamma_{m,u} = 1 - \frac{1}{1 + \zeta_{m,u} + \frac{1}{\tau_p}\text{SNR}_{m,u}^{-1}} \tag{20}$$

where $\text{SNR}_{m,u} = p_u^{(t)}\beta_{m,u}/\sigma^2$ is the *single antenna* signal to noise ratio (SNR) of UE u at AP m during the channel estimation, and

$$\zeta_{m,u} = \sum_{u' \in \mathcal{P}_u} \frac{p_{u'}^{(t)}\beta_{m,u'}}{p_u^{(t)}\beta_{m,u}} - 1 \tag{21}$$

is the relative pilot contamination level. If $\zeta_{m,u} = 0$ then there is no pilot contamination and if $\zeta_{m,u} = 0.1$ then the pilot contamination level is 10%.

The benefit of (20) is that it allows for a simple back-of-the-envelope analysis of the cancellation performance. This is illustrated in Fig. 3, which shows (a) the impact of the pilot sequence length τ_p with respect to SNR in the absence of pilot contamination and (b) the impact of SNR in the presence of pilot contamination. There are two main conclusions:

Fig. 3a): It is possible to achieve a cancellation $\gamma_{m,u}$ greater than the $\text{SNR}_{m,u}$ when the pilot length τ_p is large. This means that the interference can be pushed to below the noise floor, allowing the radar to operate optimally.

Fig. 3b): The cancellation is upper bounded by the pilot contamination at high SNRs. In particular, it holds that

$$\gamma_{m,u} = \frac{\zeta_{m,u}}{1 + \zeta_{m,u}} \leq \zeta_{m,u} \tag{22}$$

when $\text{SNR}_{m,u}$ is high. This implies that the cancellation cannot be better than the contamination level. For example, at 10%, 1% and 0.1% pilot contamination levels, the interference cancellation is limited to -10 dB, -20 dB and -30 dB.

B. Spectral division

After cancellation, the radar system processes the received data by dividing $\bar{\mathbf{y}}_m(k,l)$ with $s_n^{(r)}(k,l)$, so that

$$\mathbf{r}_{m,n}(k,l) = \frac{1}{s_n^{(r)}(k,l)}\bar{\mathbf{y}}_m(k,l) \tag{23}$$

is the radar data associated with Rx AP m and Tx AP n. A benefit of the spectral division is that it decorrelates the UE interference in time and frequency. This means that $\epsilon_{m,u}(k,l)$ is uncorrelated across the subcarriers k and symbols l.

The division also has the impact of generating one radar stream for each Tx AP. These streams can be made orthogonal with various techniques, such as by modulating $s_n^{(r)}(k,l)$ with phase ramps across the subcarriers and symbols in order to obtain orthogonality in the range-Doppler domain [16].

C. Range-Doppler processing

The range-Doppler processing is carried out by matching the signal $\mathbf{r}_{m,n}(k,l)$ against a potential target at a distance d and Doppler shift ν with the filter $w_{m,n}^{(\text{rd})}(k,l,d,\nu)$, so that

$$\bar{\mathbf{r}}_{m,n}(d,\nu) = \sum_{l=1}^{L}\sum_{k=1}^{K} w_{m,n}^{(\text{rd})}(k,l,d,\nu)\mathbf{r}_{m,n}(k,l) \tag{24}$$

is the range-Doppler map across the N antennas at Rx AP m with respect to Tx AP n.

Under the assumption of negligible clutter and that the noise and interference is approximately uncorrelated and Gaussian across the subcarriers and symbols, it holds from the signal structure (4) that the generalized likelihood ratio test (GLRT) processor is given by

$$w_{m,n}^{(\text{rd})}(k,l,d,\nu) = \frac{1}{\sqrt{KL}} e^{-j2\pi\frac{\Delta f d}{c}k} e^{j2\pi\frac{cT_p\nu}{f_c}l} \tag{25}$$

which can be implemented with the fast Fourier transform (FFT) when d and ν are evaluated in a uniform grid [14]. In practice a windowing is used to reduce the sidelobes, which amounts to a 1-3 dB SNR loss in the range and Doppler domains, depending on the window used [21].

D. Array processing

After range-Doppler processing, the signal is spatially combined across the antennas with the filter $\mathbf{w}_m(\theta)$, so that

$$\bar{r}_{m,n}(d,\nu,\theta) = \mathbf{w}_m^H(\theta)\bar{\mathbf{r}}_{m,n}(d,\nu) \tag{26}$$

is the range-Doppler-angle output of the radar processor, where θ is the steering angle. It is common to use conventional beamforming, where $\mathbf{w}_m(\theta) = \mathbf{b}_m(\theta)$. While this may work well in practice, it is suboptimal because the UE interference is correlated in the antenna dimension. Instead, one may use the GLRT combiner, which is given by

$$\mathbf{w}_m(\theta) = \frac{\mathbf{C}_m^{-1}\mathbf{b}_m(\theta)}{\sqrt{\mathbf{b}_m^H(\theta)\mathbf{C}_m^{-1}\mathbf{b}_m(\theta)}} \tag{27}$$

where $\mathbf{C}_m = \sum_{u \in \mathcal{I}_m} p_u\tilde{\mathbf{R}}_{m,u} + \sum_{u \notin \mathcal{I}_m} p_u\mathbf{R}_{m,u} + \sigma^2\mathbf{I}_N$ is the noise plus interference covariance matrix [14]. The main
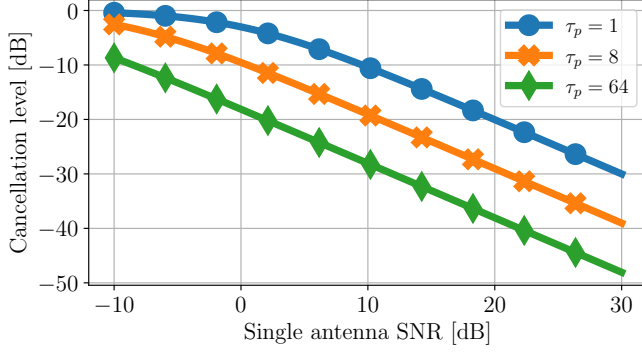
(a) Varying pilot sequence lengths τ_p when $\zeta_{m,u} = 0$.
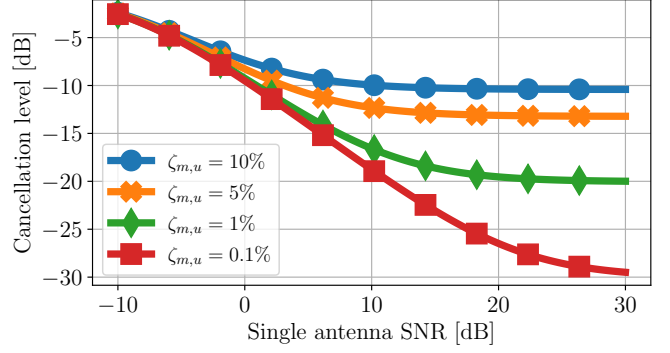
(b) Varying pilot contamination levels $\zeta_{m,u}$ when $\tau_p = 8$.

Figure 3: The reduction in UE power after interference cancellation when $N = 1$.

difference between the GLRT combiner and the conventional beamformer is that the steering vectors are pre-multiplied with the matrix inverse $\boldsymbol{C}_m^{-1}$. This has the impact of spatially mitigating the UE interference, as shown in Section VI.

In terms of computational cost, only a single set of combiners are needed since the matrices $\boldsymbol{C}_m$ are constant throughout a processing block. This implies that only a single weight calculation (27) is needed per steering angle θ, which makes the construction of the combiners negligible. The main processing cost is hence the combining (26), which should be done for each range bin d and Doppler bin ν.

E. Threshold detection

After array processing, the range-Doppler-angle output is used as a test statistic to determine the presence of a target at a distance d, Doppler velocity ν and angle θ for each pair of Rx AP m and Tx AP n. This gives the hypothesis test

$$\Lambda_{m,n}(d,\nu,\theta) = 2|\bar{r}_{m,n}(d,\nu,\theta)|^2 \underset{\mathcal{H}_0}{\overset{\mathcal{H}_1}{\gtrless}} \gamma_{m,n}^{(th)} \qquad (28)$$

where the hypothesis $\mathcal{H}_1$ indicates the presence of a target with an amplitude $\alpha_{m,n}(d,\nu,\theta) \neq 0$ and $\mathcal{H}_0$ indicates the absence of a target (i.e., $\alpha_{m,n}(d,\nu,\theta) = 0$).

By assuming that the Tx APs are orthogonally multiplexed and by neglecting the impact of clutter, the detection variable $\Lambda_{m,n}(d,\nu,\theta)$ becomes under each of the hypotheses central and non-central chi-squared distributed as

$$\Lambda_{m,n}(d,\nu,\theta) \sim \begin{cases} \chi_2^2 & \text{under } \mathcal{H}_0 \\ \chi_2^2\left(2\text{SINR}_{m,n}^{(r)}(d,\nu,\theta)\right) & \text{under } \mathcal{H}_1 \end{cases} \qquad (29)$$

as derived in [14], where under $\mathcal{H}_1$, the detection performance is characterized by the SINR, which we define as

$$\text{SINR}_{m,n}^{(r)}(d,\nu,\theta) = KL|\alpha_{m,n}(d,\nu,\theta)|^2 \qquad (30)$$
$$\times \boldsymbol{b}_{m,n}^H(\theta)\boldsymbol{C}_m^{-1}\boldsymbol{b}_{m,n,q}(\theta).$$

Note that the detector has the constant false alarm rate (CFAR) property because the distribution of $\Lambda_{m,n}(d,\nu,\theta)$ under $\mathcal{H}_0$ is independent of the noise. For a given probability of false alarm P_{FA}, the detection threshold can be evaluated as

$$\gamma_{m,n}^{(th)} = F_{m,n}^{-1}(1 - P_{\text{FA}} \,|\, \mathcal{H}_0) \qquad (31)$$

where $F_{m,n}^{-1}(P \,|\, \mathcal{H}_0)$ is the inverse cumulative distribution function (CDF) of $\Lambda_{m,n}(d,\nu,\theta)$ under $\mathcal{H}_0$. The probability of detection $P_{m,n}^{(det)}(d,\nu,\theta)$ can similarly be obtained as

$$P_{m,n}^{(det)}(d,\nu,\theta) = 1 - F_{m,n}(\gamma \,|\, \mathcal{H}_1, d, \nu, \theta) \qquad (32)$$

where $F_{m,n}(\gamma \,|\, \mathcal{H}_1, d, \nu, \theta)$ is the CDF of $\Lambda_{m,n}(d,\nu,\theta)$ under $\mathcal{H}_1$. These expressions can be used to to assess the performance of the radar system. As an example, for a value of $P_{\text{FA}} = 10^{-6}$, we get a $P_{m,n}^{(det)}(d,\nu,\theta) = 99.7\%$ when $\text{SINR}_{m,n}^{(r)}(d,\nu,\theta) \approx 15$ dB. This SINR value is used as a reference when calculating the coverage of the system in the radar simulations in Section VI.

F. Complexity analysis

The number of operations as measured by the number of multiplications and divisions *per* Rx AP *per* subcarrier *per* OFDM symbol is shown in Table I. It is assumed that the range-Doppler processing is performed over a grid of K range and L Doppler bins using FFTs. The array processing is assumed to employ N combiners. The detection block has been left out as the threshold calculations are implementation specific and often limited in complexity.

Fig. 4 shows the number of operations with respect to the number of Tx antennas $|\mathcal{T}_m|$ that are processed at each AP m when $K = 1024$, $L = 1024$, $N = 8$ and $|\mathcal{I}_m| = 8$. In order to make the numbers relatable to the communcation system, the operations are presented *relative* to the OFDM demodulation, which is assumed to operate over $K = 1024$ point FFTs. Based on these system parameters and the results in the figure, we make two remarks:

Remark 1: The range-Doppler and array processing constitute most of the operations and are approximately the same in magnitude. The UE cancellation imposes a similar load as the range-Doppler and array processing for small $|\mathcal{T}_m|$, but does not grow in complexity. In contrast, the spectral division constitutes only a fraction of the operations.

Remark 2: The radar processing is not negligible when compared to the communication system. Depending on the number of Tx APs processed, the computational cost can be more than than an order of magnitude larger than the OFDM

Table I: Number of multiplications and divisions per AP, subcarrier and OFDM symbol.

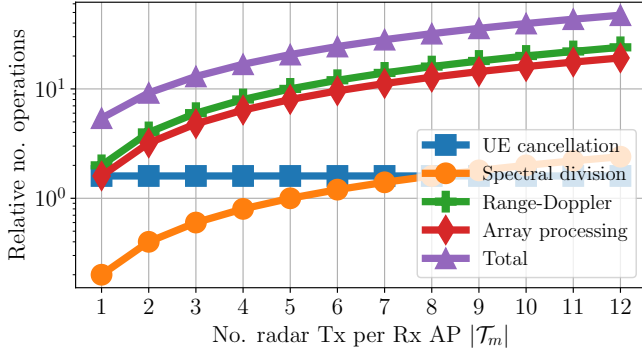| Radar signal processing block	No. operations
Interference cancellation	$\|\mathcal{I}_m\|N$
Spectral division	$\|\mathcal{T}_m\|N$
Range-Doppler processing	$\frac{1}{2}\|\mathcal{T}_m\|N\log_2(KL)$
Array processing	$\|\mathcal{T}_m\|N^2$
OFDM demodulation	$\frac{1}{2}N\log_2(K)$

Figure 4: The number of radar processing operations relative to OFDM demodulation of the algorithms in Table I when using $K = 512$, $L = 1024$, $N = 8$ and $|\mathcal{I}_m| = 8$.

demodulation. For 1, 3, 6 and 12 Tx APs, the cost is about 5, 12, 24 and 46 times the cost of OFDM demodulation.

It is worth noting that, in addition to the arithmetic operations, the processor also needs to store $KLN = 4.19 \times 10^6$ samples per Tx AP and frame, which may consume a significant amount of resources due to the memory management.

V. RESOURCE ALLOCATION

This section considers the problem of power control and Tx AP selection. The power control is necessary for balancing the communication and radar performance, while the proper selection of Tx APs is necessary to ensure an adequate radar coverage. Since both problems are coupled, we consider a two-step procedure where the selection of Tx APs is first optimized for radar performance in the absence of the communication system. The transmit powers of the UEs are then tuned to maximize the SE while constrained to inflict a limited SNR loss on the radar system. To this end, the power control is first presented, followed by the Tx AP selection.

A. Power control

In the following, we use power control as a mechanism to manage the trade-off in radar and communications performance. The scheme presented is adapted from [15] and operates by approximating $\boldsymbol{C}_m$ with the diagonal matrix

$$\frac{1}{N}\text{Tr}\{\boldsymbol{C}_m\}\boldsymbol{I}_N = \left(\sum_{u=1}^{U}\gamma_{m,u}\beta_{m,u}p_u + \sigma^2\right)\boldsymbol{I}_N \quad (33)$$

in order to evaluate the *average* interference power after interference cancellation, where $\gamma_{m,u} = 1$ if $u \neq \mathcal{I}_m$. By replacing $\boldsymbol{C}_m$ with (33) in the SINR expression (30), we get

$$\text{SINR}_{m,n}^{(r,av)}(d,\nu,\theta) = \frac{|\alpha_{m,n}(d,\nu,\theta)|^2 KLN}{\sum_{u=1}^{U}\gamma_{m,u}\beta_{m,u}p_u + \sigma^2} \quad (34)$$

which represents an average SINR that is spatially decoupled from the antenna geometry at the Rx AP. The expression $\text{SINR}_{m,n}^{(r,av)}(d,\nu,\theta)$ can be further decomposed into a SNR term and a target independent SNR loss as

$$\text{SINR}_{m,n}^{(r,av)}(d,\nu,\theta) = \frac{1}{\kappa_m}\text{SNR}_{m,n}^{(r)}(d,\nu,\theta) \quad (35)$$

where $\text{SNR}_{m,n}^{(r)}(d,\nu,\theta)$ quantifies the ideal post-processing SNR in the *absence* of the communication system

$$\text{SNR}_{m,n}^{(r)}(d,\nu,\theta) = \frac{|\alpha_{m,n}(d,\nu,\theta)|^2 KLN}{\sigma^2} \quad (36)$$

and κ_m the corresponding loss in SNR (after interference cancellation) due to the communication system

$$\kappa_m = \frac{1}{\sigma^2}\sum_{u=1}^{U}\gamma_{m,u}\beta_{m,u}p_u + 1. \quad (37)$$

The main benefit of (35) is that it decouples the radar and communication systems, allowing the impact of the UEs to be quantified by a *single* parameter κ_m at each Rx AP. As an example, if $\kappa_m = 10$ dB, then $\text{SINR}_{m,n}^{(r,av)}(d,\nu,\theta)$ will be 10 dB lower than the ideal value of $\text{SNR}_{m,n}^{(r)}(d,\nu,\theta)$.

In order to formulate the power control, κ_m is expressed as

$$\kappa_m = \boldsymbol{d}_m^T\boldsymbol{p} + 1, \quad (38)$$

where $\boldsymbol{d}_m = [\frac{1}{\sigma^2}\gamma_{m,1}\beta_{m,1},\ldots,\frac{1}{\sigma^2}\gamma_{m,U}\beta_{m,U}]^T$ and

$$\boldsymbol{p} = [p_1,\ldots p_U]^T \quad (39)$$

is the vector of power coefficients of the U UEs. Based on κ_m, one may augment any communication objective $f(\boldsymbol{p})$ by imposing (38) as additional linear constraints on the UEs as

$$\max_{\boldsymbol{p}\in\mathbb{R}^U} f(\boldsymbol{p}) \quad \text{s.t.} \quad p_{\max}\boldsymbol{1} \geq \boldsymbol{p} \geq \boldsymbol{0} \quad (40)$$

$$1 + \boldsymbol{d}_m^T\boldsymbol{p} \leq \kappa_{\max} \quad (41)$$

where $m \in \Omega/|\mathcal{T}|$ refers to the Rx APs, and $\kappa_{\max}$ is the largest tolerable radar SNR loss on the radar system and $p_{\max}$ is the largest Tx power the UEs can have. A popular objective is the sum spectral efficiency (SSE), which is given by

$$f(\boldsymbol{p}) = \sum_{u=1}^{U}\log_2(1 + \text{SINR}_u). \quad (42)$$

Since the problem is non-convex, the maximization is carried out using a local search, such as a trust-region optimizer [24].

B. Selection of Tx APs

In the following, we present a technique for selecting the Tx APs in the network. The problem is to select $|\mathcal{T}|$ Tx APs from the set of APs Ω so that the radar coverage is maximized in the *absence* of the UEs. It is assumed the Tx APs are orthogonal, so that each Tx AP to be evaluated without considering the interference from the other Tx APs.

In order to perform the selection, we let c_n denote the Tx AP selection variable as

$$c_n = \begin{cases} 1 & \text{if } n \in \mathcal{T} \\ 0 & \text{otherwise} \end{cases} \tag{43}$$

where $c_n = 1$ means that AP n is a Tx AP (and otherwise a Rx AP). This allows the SNR between any pair of Tx AP n and Rx AP m to be expressed as

$$\overline{\text{SNR}}_{m,n}^{(r)}(\boldsymbol{c}, d, \nu, \theta) = c_n(1 - c_m)\text{SNR}_{m,n}^{(r)}(d, \nu, \theta). \tag{44}$$

In order to evaluate the coverage, we will consider the pair of Tx and Rx APs with the highest SNR. This serves as a *lower bound* on the detection performance and gives the SNR defined by

$$\text{SNR}_{\text{max}}(\boldsymbol{c}, d, \nu, \theta) = \max_{m,n} \overline{\text{SNR}}_{m,n}^{(r)}(\boldsymbol{c}, d, \nu, \theta) \tag{45}$$

where $\boldsymbol{c} = [c_1, \ldots, c_M]$ is the selection vector. The lower bounding is due to the equivalence with the probability of detection, as the SINR uniquely defines (29) under $\mathcal{H}_1$.

By discretizing the parameter space into a set of Q_{rt} reference targets with parameters d_q, ν_q and θ_q, we define the *coverage* of the radar system as the fraction of targets that exceeds a minimum SNR. This gives the coverage

$$g(\boldsymbol{c}) = \frac{1}{Q_{\text{rt}}} \sum_{q=1}^{Q_{\text{rt}}} \mathcal{Q}\left(\frac{\text{SNR}_{\text{max}}(\boldsymbol{c}, d_q, \nu_q, \theta_q)}{\text{SNR}_{\text{min}}}\right) \tag{46}$$

where SNR_{min} is the threshold and $\mathcal{Q}(x)$ is a one-bit quantizer, where $\mathcal{Q}(x) = 1$ if $x \geq 1$ and zero otherwise. The selection is consequently formulated to maximize the coverage as

$$\max_{\boldsymbol{c} \in \{0,1\}^M} g(\boldsymbol{c}) \tag{47}$$

$$\text{s.t. } \mathbf{1}^T \boldsymbol{c} = |\mathcal{T}| \tag{48}$$

where (48) ensures that exactly $|\mathcal{T}|$ Tx APs are selected. Since the problem is combinatorial and difficult to solve optimally, we will consider the suboptimal, but computationally efficient, scheme presented in Algorithm 1. This algorithm operates by iteratively adding one Tx AP to $\mathcal{T}$ so that $g(\boldsymbol{c})$ is maximized at each iteration, given the previously added Tx APs, until a total of $|\mathcal{T}|$ Tx APs have been selected.

Since the cost function $g(\boldsymbol{c})$ requires the evaluation of $|\alpha_{m,n}(d, \nu, \theta)|^2$ in order to assess the SNR of the reference targets, we will make use of the radar range equation

$$|\alpha_{m,n}(d, \nu, \theta)|^2 = \frac{G^2 \lambda^2 \sigma_{m,n}}{64\pi^3 d_m^2(d,\theta) d_n^2(d,\theta)} \tag{49}$$

where G is the Tx and Rx antenna gains, $\sigma_{m,n}$ the bistatic radar cross section (RCS) and $d_m(d,\theta)$ the distance between AP m and the target location [21]. In the evaluation of

---

Algorithm 1 Greedy algorithm for selecting Tx APs.

1: Initialize $\mathbf{c} = \mathbf{0}$
2: **for** $i = 1$ to $|\mathcal{T}|$ **do**
3:      **for** $m = 1$ to M **do**
4:          Set $g_m = 0$
5:          **if** $c_m = 0$ **then**
6:              Set $c_m = 1$
7:              Set $g_m = g(\mathbf{c})$
8:              Set $c_m = 0$
9:          **end if**
10:      **end for**
11:      Set $m^* = \text{argmax}_m \ g_m$
12:      Set $c_{m^*} = 1$
13: **end for**
14: Return $\mathbf{c} = [c_1, \ldots, c_M]^T$

Table II: The base parameters used in the simulations. (a) The 6 dB are set to account for signal processing losses.

Parameter	Notation	Value	Unit
Coverage area		500×500	m^2
No. APs	M	32	
No. UEs	U	40	
No. antennas per AP	N	8	
Carrier frequency	f_c	6	GHz
Subcarrier spacing	Δf	120	kHz
No. subcarriers	K	1024	
Bandwidth	$K\Delta f$	122.88	MHz
No. OFDM symbols	L	1024	
No. pilots	τ_p	20	
AP height		5	m
UE height		1	m
Target height		1	m
Tx/Rx gain	G	0	dBi
Radar cross section	$\sigma_{m,n}$	0	dBsm
Noise figure	N_f	12+6[a]	dB
Angular standard deviation	σ_{az}	5	degrees
Decorrelation distance		9	m
Shadow fading standard deviation		4	dB

$|\alpha_{m,n}(d, \nu, \theta)|^2$, one may for example use a RCS of a pedestrian or some other reference object. Note that the Tx power has been omitted from (49) as it is factored out in (2).

VI. NUMERICAL RESULTS

A. Simulation setup

In the following, we evaluate the system by using numerical simulations. The base parameters are listed in Table II.

We consider a 500×500 m coverage area where $M = 32$ APs with $N = 8$ antennas and $U = 40$ UEs are placed at random locations. This corresponds to 128 APs per km^2 and 160 UEs per km^2. The APs and UEs are located at a height of 5 m and 1 m above the ground. The carrier frequency is
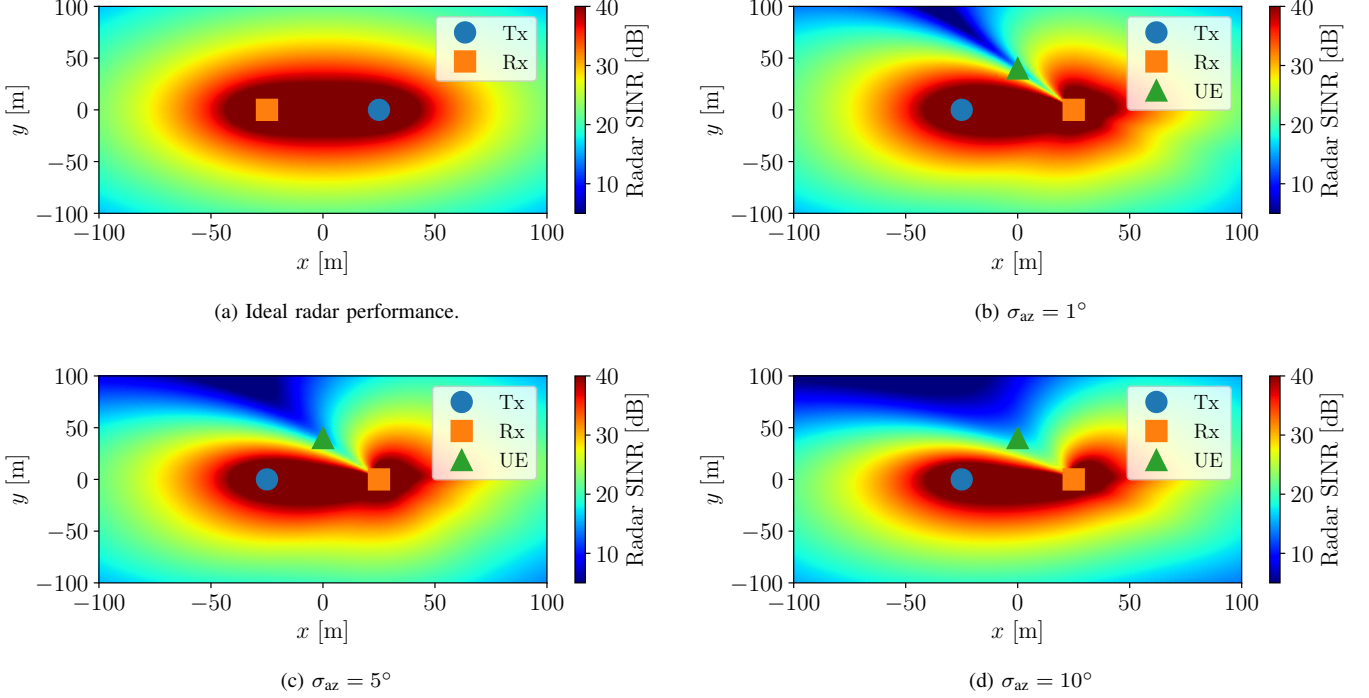
Figure 5: Illustration of the channel model from the perspective of the radar system. Because the UE channels are spatially directional, the interference causes low SINR regions, where the spatial extent is determined by the angular spread σ_{az}.

set to $f_c = 6$ GHz and $K = 1024$ subcarriers are used with $\Delta f = 120$ kHz, giving a bandwidth of $K\Delta f = 122.88$ MHz. This corresponds to a fractional bandwidth of 2%. A frame is set to consist of $L = 1024$ OFDM symbols and the targets are modeled to have a bistatic RCS of 0 dBsm and a height of 1 m above the ground. Note that the the coverage area is not wrapped as in [25], meaning that cell-edge effects are present.

In order to estimate the channels, a pilot sequence length of $\tau_p = 20$ is used, corresponding to 50% of the number of UEs. The pilots are assigned across the UEs and Tx APs by using the greedy pilot assignment algorithm in [2]. During the channel estimation, the UEs are set to transmit with 30 dBm and the Tx APs with 20 dBm.

All antennas are assumed isotropic with a Tx and Rx gain of $G = 0$ dBi. The Tx APs are set to transmit with a constant power of $p_t = 20$ dBm and the UEs with a maximum power of $p_{\text{max}} = 30$ dBm. The noise power σ^2 is modeled as

$$\sigma^2 = k_B T K \Delta f N_f \tag{50}$$

where k_B is Boltzmann's constant, $T = 300$ K is the noise temperature and $N_f = 12 + 6 = 18$ dB is the noise figure, where the 6 dB is added to account for various signal processing losses [21].

The LSF coefficients $\beta_{m,u}$ are modeled by using the 3GPP urban micro-cell model as in [23], using a shadow fading standard deviation of 4 dB and a decorrelation distance of 9 m. To model the covariance matrices $\boldsymbol{R}_{m,u}$, we use the local scattering model with a Gaussian distribution presented in [2], but extended to arbitrary antenna configurations. This gives the generalized expression

$$\boldsymbol{R}_{m,u} = \frac{\beta_{m,u}}{\sqrt{2\pi}\sigma_{\text{az}}} \int e^{-\frac{(\theta - \theta_{m,u})^2}{2\sigma_{\text{az}}^2}} \boldsymbol{b}_m(\theta)\boldsymbol{b}_m^H(\theta)d\theta \tag{51}$$

where σ_{az} is the angular standard deviation. In the simulations, we use a uniform circular array in order to simulate a 360 degree coverage surrounding the APs.

The channel model is visualized in Fig. 5, which shows the SINR of the radar system for various σ_{az} in the absence of interference cancellation, where the UE transmits with $p_u = 30$ dBm. Fig. 5 (a) shows the SINR map in the absence of UE interference, while (b), (c) and (d) shows the SINR map for $\sigma_{\text{az}} = 1$, 5 and 10 degrees. As can be seen, the impact of the UE is a spatially directive interference that introduces a blind region in the radar image. By increasing σ_{az}, the width of the blind region is increased. This is because σ_{az} models the spatial spread of the multipath components of the UE channel, which competes with the backscattered echoes of the radar system. For $\sigma_{\text{az}} = 1$, the interference is a notch, while increasing to a quadrant when $\sigma_{\text{az}} = 10$. As a middle ground, we will in the simulations use $\sigma_{\text{az}} = 5$ degrees.

B. Monte-Carlo simulations

In the following, we use Monte-Carlo simulations to evaluate the SE of the communication system and the coverage of the radar system. Centralized MMSE combining is used across all Rx APs in order to process the UEs. In order to evaluate the radar system, we set the Rx APs to process the Tx APs that are within 100 m. For calculating the radar coverage, we use $\text{SINR}_{min}^{(r)} = 15$ dB, which corresponds to a probability
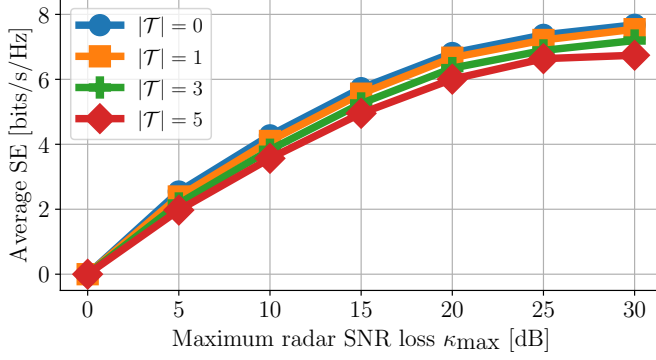
(a) Average SE versus $\kappa_{\max}$.
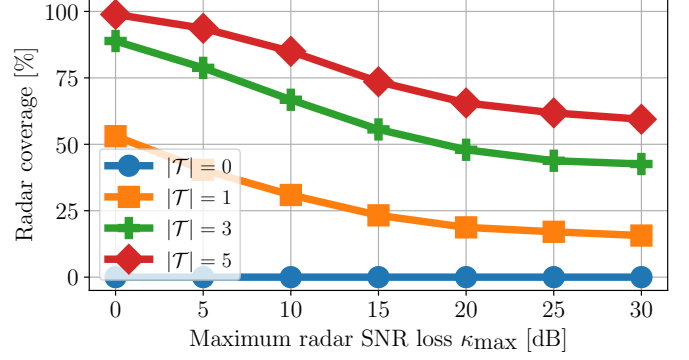
(b) Radar coverage

Figure 6: Performance curves for various Tx APs $|\mathcal{T}|$ and power control trade-offs $\kappa_{\max}$ in the *absence* of interference cancellation (i.e., $|\mathcal{I}_m| = 0$). As can be seen, increasing the performance on either system results in a substantial performance loss on the other. As shown in Fig. 7, the interference cancellation provides the additional margin needed to close the gap.
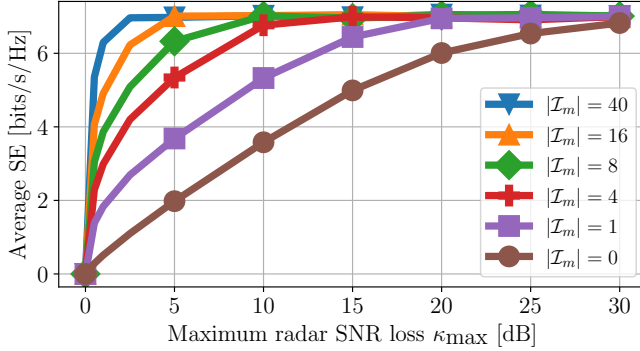

Figure 7: The per UE average SE versus the SNR loss $\kappa_{\max}$ when using $|\mathcal{T}| = 5$. The number of UEs cancelled $|\mathcal{I}_m|$ improves the SE because the UEs can transmit with more power while imposing the same SNR loss on the radar system.

of detection of approximately 99.7% at $P_{\mathrm{FA}} = 10^{-6}$ when using (31) and (32). A total of 200 Monte-Carlo simulations are carried out for each data point.

The results are illustrated in Fig. 6, Fig. 7 and Fig. 8 and are summarized as follows:

Key points of Fig. 6: The figure shows (a) the average SE across all UEs and (b) radar coverage for different number of Tx APs $|\mathcal{T}|$ and power control coefficients $\kappa_{\max}$ in the absence of interference cancellation.

The results in (a) and (b) show that both $|\mathcal{T}|$ and $\kappa_{\max}$ have a substantial impact of the performance. A large $|\mathcal{T}|$ implies a large number of radar transmitters but fewer Rx APs for receiving UE signals. This increases the radar coverage at the cost of increased pilot contamination and spatial degrees of freedom in the MMSE combining as the effective number of UEs (i.e., Tx APs) increases. This can be seen in (a), where the the SE reduces with increasing $|\mathcal{T}|$ and in (b) where the radar coverage increases with $|\mathcal{T}|$. Similarly, a small $\kappa_{\max}$ imply a small SNR loss on the radar system, at the cost of constraining

the UEs to transmit with low power and hence operate at a small SE. By increasing $\kappa_{\max}$, the SE increases at the cost of radar coverage. This can be seen in (a) where the SE is zero when $\kappa_{\max} = 0$ and monotonically increasing as $\kappa_{\max}$ increases, and in (b) where the radar coverage decreases with increasing $\kappa_{\max}$.

From (b), we observe that $|\mathcal{T}| = 5$ Tx APs is enough to provide full 98.9% radar coverage when there is no UE interference present ($\kappa_{\max} = 0$ dB). This drops to around 59.5% when $\kappa_{\max} = 30$ dB as $\kappa_{\max}$ determines the amount of power the UEs can transmit. From (a), we measure a SE of 1.97, 4.94 and 6.74 bits/s/Hz for $|\mathcal{T}| = 5$ when using the power control coefficients $\kappa_{\max} = 5$, 15 and 30 dB.

Interestingly, the UE performance is not adversely impacted by the number of Tx APs. This is because of the inherent redundancy in the communication system, as the number of antennas is much larger than the number of UEs. By defining the system load as the number of Tx antennas divided by the number Rx antennas, we get the expression

$$\mathcal{L} = \frac{U + |\mathcal{T}|}{N(M - |\mathcal{T}|)} \tag{52}$$

which gives a load of $\mathcal{L} = 15.6\%$ when $|\mathcal{T}| = 0$ and a load of $\mathcal{L} = 20.8\%$ when $|\mathcal{T}| = 5$, corresponding to an 33.3% increase in total load. This is the main reason for the loss in communication performance when $|\mathcal{T}|$ increases. At $\kappa = 30$ dB, the SE is 7.68 bits/s/Hz when $|\mathcal{T}| = 0$ and 6.74 bits/s/Hz when $|\mathcal{T}| = 5$. This corresponds to a loss of 12.2% in average SE, which aligns with the 33.3% increase in system load.

Note that the system load is primarily increased because of the relatively small number of APs M and large number of antennas N per AP. This means that each Tx AP results in a loss of $N = 8$ antennas. The performance can obviously be improved by adjusting the ratio M/N.

The results in (a) and (b) show that both systems can operate simultaneously, but with a large deviation from optimal performance. This is mainly due to the power control coefficient

(a) $\kappa_{\max} = 20$ dB and $|\mathcal{I}_m| = 0$

(b) $\kappa_{\max} = 13$ dB and $|\mathcal{I}_m| = 1$

(c) $\kappa_{\max} = 4.5$ dB and $|\mathcal{I}_m| = 8$
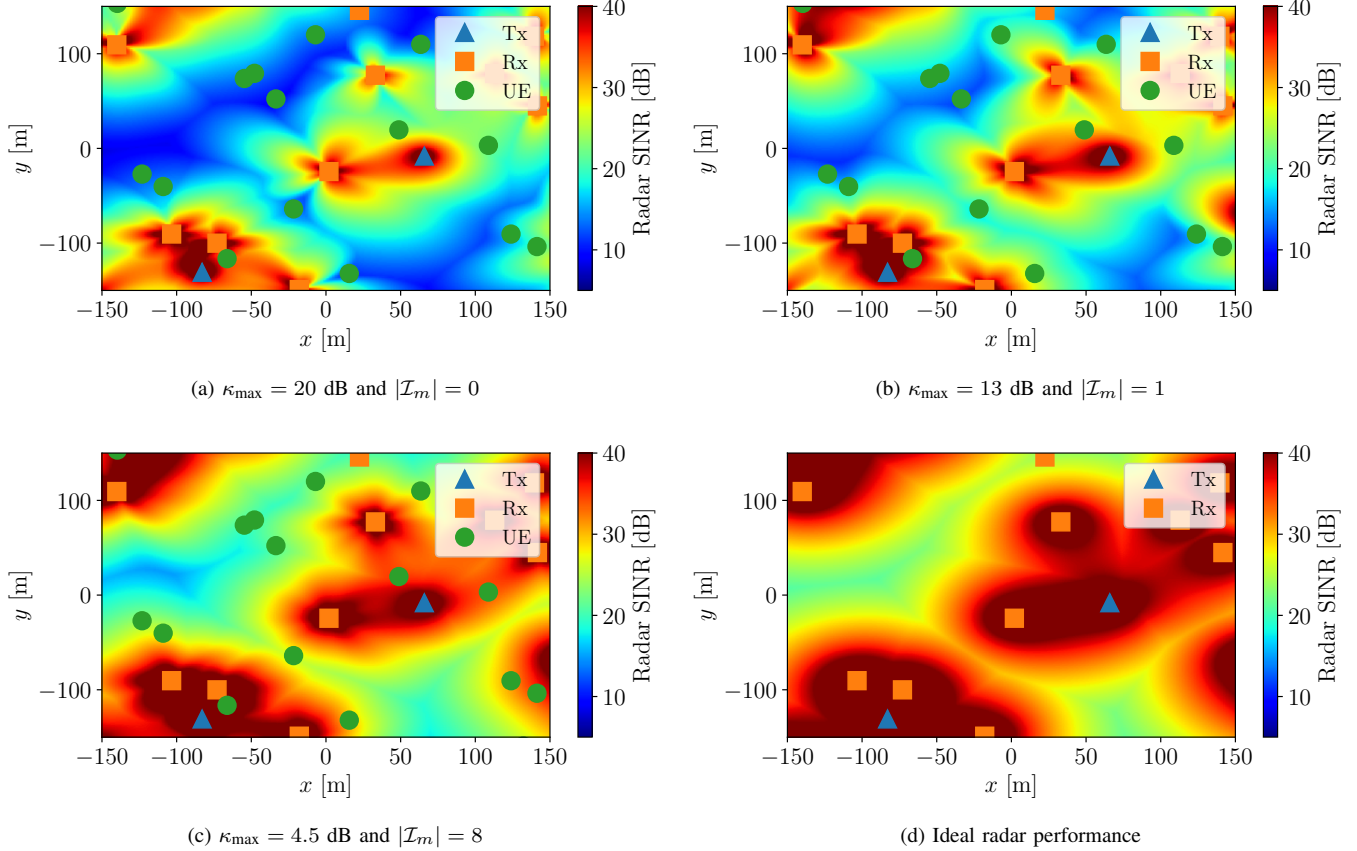
(d) Ideal radar performance

Figure 8: Radar SINR maps obtained using (45) for various system parameters. The configurations in (a), (b) and (c) have the same SE and differ only in the signal processing and the power control, illustrating the impact of the radar processing.

$\kappa_{\max}$. As we show next, the interference cancellation provides the margin needed to operate closer to optimum.

Key points of Fig. 7: The figure shows the average SE for different number of UEs $|\mathcal{I}_m|$ cancelled at the Rx APs when using $|\mathcal{T}| = 5$ Tx APs. In order to construct $\mathcal{I}_m$, we use an ordered cancellation scheme where the UEs are sorted with respect to their largest LSF coefficients and cancelled in that order. This means that if $|\mathcal{I}_m| = 4$, then the four UEs with the largest LSF are cancelled at Rx AP m.

The figure illustrates how the processing at the radar system is coupled with the communication system. As can be seen, the SE increases rapidly with $|\mathcal{I}_m|$. For example, at $\kappa_{\max} = 5$ dB, we measure a SE of 1.96 bits/s/Hz when $|\mathcal{I}_m| = 0$ and 3.66 bits/s/Hz when $|\mathcal{I}_m| = 1$, which corresponds to a 87% increase in SE. When $|\mathcal{I}_m| = 4$ and $|\mathcal{I}_m| = 8$, the SE is increased to 5.37 and 6.28 bits/s/Hz, which corresponds to a 20.3% and 6.8% deviation from the ideal SE when $|\mathcal{T}| = 5$, and a 30% and 18.2% deviation when $|\mathcal{T}| = 0$ (i.e., when there is no radar system). For each configuration, the radar coverage is measured to 93.5% from Fig. 6, as the SNR loss $\kappa_{\max}$ is the same. Interestingly, when all UEs are canceled (i.e., $|\mathcal{I}_m| = 40$), the system operates nearly optimally at $\kappa_{\max} = 5$ dB with a SE of 7.01 bits/s/Hz, which corresponds to a loss of $1 - 7.01/7.68 = 8.7$ % in SE. This indicates a trade-off between the amount of computations allocated for interference

cancellation and the final system performance.

These results indicate that the system is capable of operating both radar *and* communications with a performance that is close to optimal. For example, when $|\mathcal{T}| = 5$, $\kappa_{\max} = 5$ dB and $|\mathcal{I}_m| = 8$, then the system can operate with a 93.5% radar coverage at a cost of 18.2% in average SE. Increasing the UE cancellation to $|\mathcal{I}_m| = 16$ gives the same coverage (as the SNR loss is the same) at a 9.1% loss in SE.

Key points of Fig. 8: The figure visualizes a realization of the SINR map of the radar system when using (a) $\kappa_{\max} = 20$ dB and $|\mathcal{I}_m| = 0$, (b) $\kappa_{\max} = 13$ dB and $|\mathcal{I}_m| = 1$, (c) $\kappa_{\max} = 4.5$ dB and $|\mathcal{I}_m| = 8$, and (d) ideal performance. The SINR maps were obtained by using (47) and $|\mathcal{T}| = 5$.

As can be seen from Fig. 7, each of the systems in (a), (b) and (c) have the same SE and differ only in the signal processing and power control. By comparing (a) with (b) and (c), it holds from $\kappa_{\max}$ that the cancellation provides a 7 dB and 15.5 dB SINR improvement, which emphasizes the importance of the interference cancellation. By comparing (c) with (d), it can be seen that the radar system operates nearly optimally in terms of coverage despite communicating with the UEs.

C. Qualitative analysis

In the previous sections, we have demonstrated an integration of a radar system with 93.5% coverage (or 5 dB SNR

(a) The SINR map of the right Rx AP.

(b) The SINR map of the left Rx AP.

(c) The combined SINR map using (45).

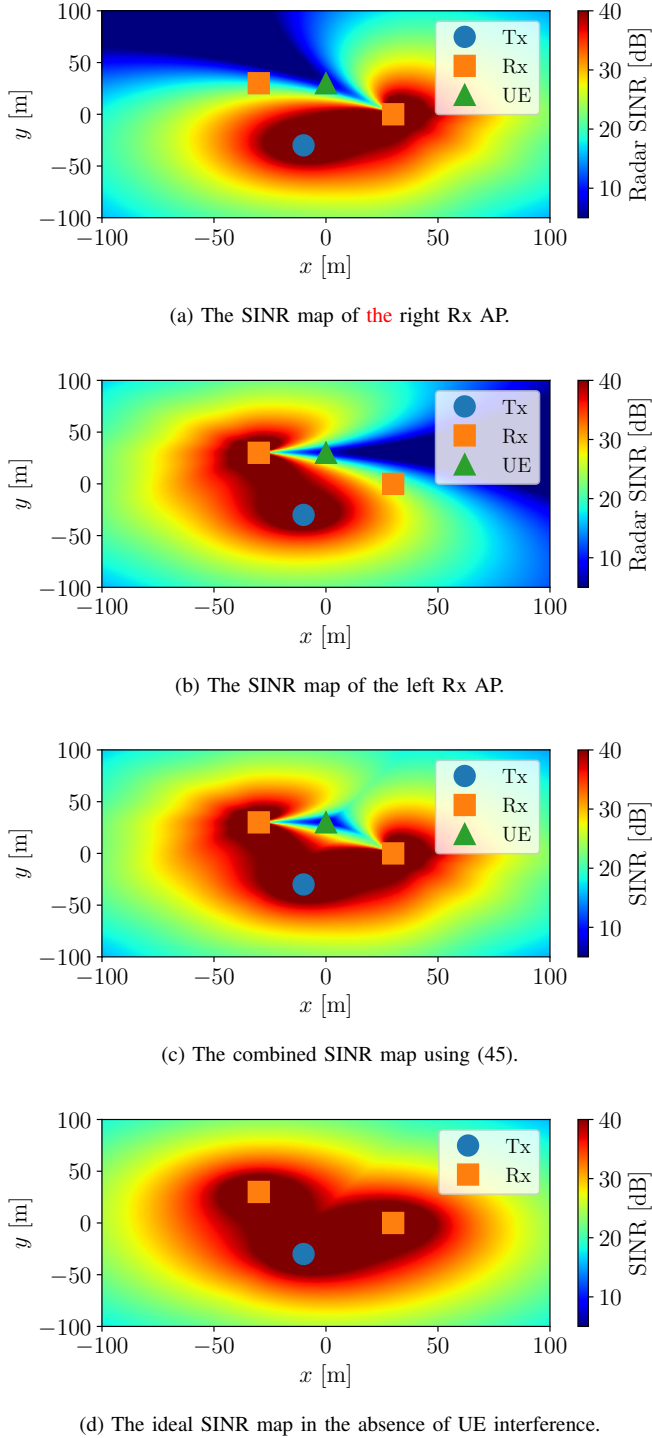(d) The ideal SINR map in the absence of UE interference.

Figure 9: An illustration of spatial diversity in radar networks. The diversity in aspect angles allows for almost complete coverage despite the spatially directive interference.

loss) into a cell-free architecture, at a cost of 8.7 to 18.2% in SE. In the following, we briefly outline the key techniques that enable the integration.

From the communication perspective, the main parameter is the spatial degree of freedom due to the large number of distributed antennas. This allows the additional Tx APs to be accommodated by the remaining APs by utilizing spatial combining, as if the Tx APs would be conventional UEs. In this sense, each Tx AP is handled by the network as "another scheduled UE", which explains why the integration works.

The radar system, on the other hand, is different from the communication system as it needs to provide a wide area coverage with a challenging link budget. This means that spatial combining is *not* sufficient to mitigate the UE interference. In fact, it appears that the main challenge is to mitigate the interference imposed on the radar system, and not vice versa. To this end, the radar performance can be attributed to a combination of five techniques, being large processing gains, adaptive beamforming, spatial diversity, interference cancellation and power control. All methods together can under some circumstances provide more than 100 dB in mitigation, which is key for realizing the radar system. These techniques are individually summarized as follows:

Processing gain: In contrast to the UEs, the radar operates by integrating a large number of subcarriers and symbols in order to determine the presence of a potential target. This provides a spreading gain that suppresses the noise and UE interference. This can be seen in e.g., (34), which shows that the radar processing provides a SINR improvement of KLN, which can be made large in practice. For the configuration in Table II, this corresponds to a SINR improvement of $10\log_{10}(1024 \cdot 1024 \cdot 8) = 69$ dB!

Adaptive beamforming: The matrix inversion $\mathbf{C}^{-1}$ in the combining filters (27) provides a layer of spatial discrimination against the UE interference. This is illustrated in Fig. 5 and is possible due to the spatial correlation of the UE channels. The consequence is that the UE interference is focused along a direction in space, which allows targets to be detected at the areas unaffected by the interference.

Spatial diversity: The distributed deployment further mitigates the UE interference when combined with adaptive beamforming. This is attributed to the aspect angle diversity, which allows the interference to be spatially focused, as illustrated in Fig. 9. Both APs in (a) and (b) have significant blind regions due to the interference, but when combined in (c), the interference is focused around the UE, which retains significant portions of the field of view. When compared with the ideal performance in (d), most of the coverage is retained except around a focused spot at the location of the UE.

Although the interference can also be mitigated with coherent processing across the APs, the results emphasize that coherent processing is *not* a pre-requisite for this type of spatial focusing. This means hardware restricted implementations can also benefit significantly from distributed architectures.

Interference cancellation: The interference cancellation provides another layer of mitigation. By reconstructing the UE signals from the channel and payload estimates, the interference can be subtracted in the subcarrier domain. As shown in Fig. 3 (and Fig. 7), the cancellation can provide tens of decibel in interference reduction depending on the pilot contamination and number of training samples used.

Power control: The power control is used as a final method to balance the trade-offs between the radar and communication performance. This is accomplished by tuning the power coefficients of the UEs to maximize the SE while limiting the SNR

loss in the radar system. The power control takes into account the radar signal processing and allows the performance to be adjusted to the signal conditions at hand.

VII. Conclusion

This paper has presented a cell-free communication system with an uplink radar system integration. The system operates by splitting the access points (APs) into transmitting (Tx) APs and receiving (Rx) APs. The Tx APs transmit dedicated signals for sensing while the Rx AP receive both the radar and communication signals. Since the Tx APs behave like conventional UEs, the corresponding increase in system load is handled *natively* with multiuser MIMO at the Rx APs.

In order to mitigate the UE interference imposed on the radar system, a combination of large processing gains, adaptive beamforming, spatial diversity, power control and interference cancellation is used. For the scenario considered, we show that the added computations needed to implement the radar is in the order of 10 times the orthogonal frequency division multiplexing (OFDM) demodulation of the communication system, being reasonable for practical implementations.

The system is validated numerically by using Monte-Carlo simulations in order to evaluate the trade-offs in radar and communication performance, where a 93.5% *per-frame* radar coverage at the cost of 8.7 to 18.2% in spectral efficiency is reported when cancelling at least 8 UEs in a 500×500 meter service area consisting of 32 APs and 40 UEs at random locations. This pairs with recent works in cell-free systems that employ downlink beamformers for sensing, as the system enables the detections acquired in the uplink to be utilized for steering the sensing beamformers in the downlink for tracking. To this end, the proposed integration serves as a promising candidate for enabling radar in future cell-free networks.

VIII. Acknowledgments

References

[1] G. Interdonato, E. Björnson, H. Q. Ngo, P. Frenger, and E. G. Larsson, "Ubiquitous cell-free Massive MIMO communications," *EURASIP Journal on Wireless Communications and Networking*, vol. 2019, no. 1, aug 2019.

[2] Özlem Tugfe Demir, E. Björnson, and L. Sanguinetti, "Foundations of User-Centric Cell-Free Massive MIMO," *Foundations and Trends in Signal Processing*, vol. 14, no. 3-4, pp. 162–472, 2021.

[3] A. Zhang, M. L. Rahman, X. Huang, Y. J. Guo, S. Chen, and R. W. Heath, "Perceptive Mobile Networks: Cellular Networks With Radio Vision via Joint Communication and Radar Sensing," *IEEE Vehicular Technology Magazine*, vol. 16, no. 2, pp. 20–30, 2021.

[4] F. Liu, Y. Cui, C. Masouros, J. Xu, T. X. Han, Y. C. Eldar, and S. Buzzi, "Integrated Sensing and Communications: Toward Dual-Functional Wireless Networks for 6G and Beyond," *IEEE Journal on Selected Areas in Communications*, vol. 40, no. 6, pp. 1728–1767, 2022.

[5] Z. Behdad, O. T. Demir, K. W. Sung, E. Bjornson, and C. Cavdar, "Power Allocation for Joint Communication and Sensing in Cell-Free Massive MIMO," in *GLOBECOM 2022 - 2022 IEEE Global Communications Conference*, 2022, pp. 4081–4086.

[6] ——, "Multi-Static Target Detection and Power Allocation for Integrated Sensing and Communication in Cell-Free Massive MIMO," 2023.

[7] U. Demirhan and A. Alkhateeb, "Cell-Free ISAC MIMO Systems: Joint Sensing and Communication Beamforming," 2023.

[8] Y. Y. Chu, M. Shakiba-Herfeh, M. Kamoun, E. Grossi, and S. Buzzi, "Integrated Sensing and Communication in User-Centric Cell-Free Massive MIMO Systems with OFDM Modulation," in *2023 IEEE 34th Annual International Symposium on Personal, Indoor and Mobile Radio Communications (PIMRC)*, 2023.

[9] S. Liu, R. Liu, M. Li, and Q. Liu, "Cooperative Cell-Free ISAC Networks: Joint BS Mode Selection and Beamforming Design," 2023.

[10] M. Elfiatoure, M. Mohammadi, H. Q. Ngo, and M. Matthaiou, "Cell-Free Massive MIMO for ISAC: Access Point Operation Mode Selection and Power Control," 2023.

[11] I. W. G. da Silva, D. P. M. Osorio, and M. Juntti, "Multi-Static ISAC in Cell-Free Massive MIMO: Precoder Design and Privacy Assessment," 2023.

[12] Z. Ren, J. Xu, L. Qiu, and D. W. K. Ng, "Secure Cell-Free Integrated Sensing and Communication in the Presence of Information and Sensing Eavesdroppers," 2023.

[13] Z. Behdad, O. T. Demir, K. W. Sung, and C. Cavdar, "Joint Processing and Transmission Energy Optimization for ISAC in Cell-Free Massive MIMO with URLLC," 2024.

[14] A. Sakhnini, M. Guenach, A. Bourdoux, H. Sahli, and S. Pollin, "A Target Detection Analysis in Cell-Free Massive MIMO Joint Communication and Radar Systems," in *ICC 2022 - IEEE International Conference on Communications*, 2022, pp. 2567–2572.

[15] A. Sakhnini, A. Bourdoux, M. Guenach, H. Sahli, and S. Pollin, "Uplink Payload Power Control in Cell-Free Communication and Radar Networks," in *GLOBECOM 2022 - 2022 IEEE Global Communications Conference*, 2022, pp. 5111–5116.

[16] A. Sakhnini, A. Bourdoux, and S. Pollin, "Range-Doppler Division Multiple Access for Joint Radar and Communication," in *2023 IEEE International Conference on Communications (ICC): SAC Integrated Sensing and Communication Track (IEEE ICC'23 - SAC-13 ISAC Track)*.

[17] Y. Cao and Q.-Y. Yu, "Joint Resource Allocation for User-Centric Cell-Free Integrated Sensing and Communication Systems," *IEEE Communications Letters*, vol. 27, no. 9, pp. 2338–2342, 2023.

[18] ——, "Design and Performance Analyses of V-OFDM Integrated Signal for Cell-Free Massive MIMO Joint Communication and Radar System," *IEEE Systems Journal*, vol. 17, no. 4, pp. 5943–5954, 2023.

[19] S. Rivetti, E. Bjornson, and M. Skoglund, "Secure Spatial Signal Design for ISAC in a Cell-Free MIMO Network," 2024.

[20] A. Sakhnini, A. Bourdoux, and S. Pollin, "Estimation of Array Locations, Orientations, Timing Offsets and Target Locations in Bistatic Radars," *IEEE Transactions on Radar Systems*, vol. 1, pp. 520–531, 2023.

[21] M. A. Richards, J. A. Scheer, and W. A. Holm, Eds., *Principles of Modern Radar: Basic principles*. Institution of Engineering and Technology, jan 2010.

[22] E. Björnson, L. Sanguinetti, and M. Debbah, "Massive MIMO with imperfect channel covariance information," in *2016 50th Asilomar Conference on Signals, Systems and Computers*, 2016, pp. 974–978.

[23] E. Björnson and L. Sanguinetti, "Making Cell-Free Massive MIMO Competitive With MMSE Processing and Centralized Implementation," *IEEE Transactions on Wireless Communications*, vol. 19, no. 1, pp. 77–90, 2020.

[24] J. Nocedal and S. Wright, *Numerical Optimization*, ser. Springer Series in Operations Research and Financial Engineering. Springer New York, 2006.

[25] H. Q. Ngo, A. Ashikhmin, H. Yang, E. G. Larsson, and T. L. Marzetta, "Cell-Free Massive MIMO Versus Small Cells," *IEEE Transactions on Wireless Communications*, vol. 16, no. 3, pp. 1834–1850, mar 2017.